Journal of
Synchrotron
Radiation

ISSN 1600-5775

Received 23 August 2014
Accepted 25 October 2014

Polytypism in GaAs nanowires: determination of the interplanar spacing of wurtzite GaAs by X-ray diffraction

Martin Köhl,[a]* Philipp Schroth,[a] Andrey A. Minkevich,[a] Jean-Wolfgang Hornung,[a] Emmanouil Dimakis,[b,c] Claudio Somaschini,[b] Lutz Geelhaar,[b] Timo Aschenbrenner,[d,e] Sergey Lazarev,[a] Daniil Grigoriev,[f] Ullrich Pietsch[g] and Tilo Baumbach[a,d,f]

[a]Institute for Photon Science and Synchrotron Radiation, Karlsruhe Institute of Technology, Hermann-von-Helmholtz-Platz 1, 76344 Eggenstein-Leopoldshafen, Germany, [b]Paul-Drude-Institut für Festkörperelektronik, Hausvogteiplatz 5-7, 10117 Berlin, Germany, [c]Helmholtz-Zentrum Dresden-Rossendorf, Bautzner Landstrasse 400, 01328 Dresden, Germany, [d]ANKA, Karlsruhe Institute of Technology, Hermann-von-Helmholtz-Platz 1, 76344 Eggenstein-Leopoldshafen, Germany, [e]Institute of Solid State Physics/Semiconductor Epitaxy, University of Bremen, Otto-Hahn-Allee NW1, 28359 Bremen, Germany, [f]Laboratory for Application of Synchrotron Radiation, Karlsruhe Institute of Technology, Kaiserstrasse 12, 76131 Karlsruhe, Germany, and [g]Solid State Physics, University of Siegen, 57068 Siegen, Germany. *E-mail: martin.koehl@kit.edu

In GaAs nanowires grown along the cubic $[111]_c$ direction, zinc blende and wurtzite arrangements have been observed in their stacking sequence, since the energetic barriers for nucleation are typically of similar order of magnitude. It is known that the interplanar spacing of the $(111)_c$ Ga (or As) planes in the zinc blende polytype varies slightly from the wurtzite polytype. However, different values have been reported in the literature. Here, the ratio of the interplanar spacing of these polytypes is extracted based on X-ray diffraction measurements for thin GaAs nanowires with a mean diameter of 18–25 nm. The measurements are performed with a nano-focused beam which facilitates the separation of the scattering of nanowires and of parasitic growth. The interplanar spacing of the $(111)_c$ Ga (or As) planes in the wurtzite arrangement in GaAs nanowires is observed to be 0.66% $\pm$ 0.02% larger than in the zinc blende arrangement.

Keywords: GaAs; nanowires; polytypism; X-ray diffraction; nanofocus.

1. Introduction

Polytypism in GaAs nanowires refers to the simultaneous occurrence of regions arranged in zinc blende and wurtzite structure inside a single nanowire grown in the (cubic) $[111]_c$ direction (Koguchi *et al.*, 1992; Dick *et al.*, 2010). This atomic arrangement has strong influence on the optical and electronic properties (Bao *et al.*, 2008; Spirkoska *et al.*, 2009; Hjort *et al.*, 2013) of the grown nanowires. Control of this polytypism is therefore essential for tailoring the properties of nanowires for current and future applications (Hayden *et al.*, 2008; Tomioka *et al.*, 2011) such as transistors (Xiang *et al.*, 2006; Tomioka *et al.*, 2012), lasing (Duan *et al.*, 2003; Saxena *et al.*, 2013), solar cells (Tian *et al.*, 2007), thermoelectric materials (Hochbaum *et al.*, 2008) and sensors (Cui *et al.*, 2001; Stern *et al.*, 2007). In addition, nanowires proved valuable also for fundamental research, for example on qubits (Cartwright, 2010), single photon sources (Reimer *et al.*, 2012) and even research on Majorana fermions (Mourik *et al.*, 2012).

Most importantly, it is well established that these atomic arrangements, which are illustrated in Fig. 1, vary slightly in their lattice constants. However, different values for these

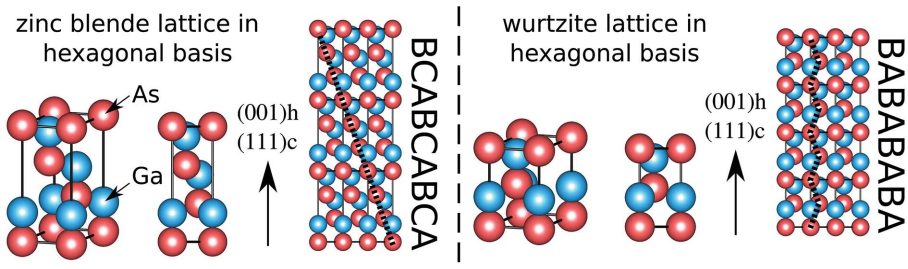

Figure 1
Illustration of the zinc blende and wurtzite arrangement.

Table 1
Summary of the published values d_{WZ}/d_{ZB} in GaAs.

All nanowire samples have been grown by molecular beam epitaxy. No dopants have been added to the nanowires (apart from possibly catalyst atoms). Δ refers to the diameter of the nanowires, l to their length. S refers to the substrate (NO = native oxide layer; BL = buffer layer; R = oxide layer removed), C to the catalyst, T to the substrate temperature during growth and M to the measurement technique (LXRD = XRD with laboratory source; SXRD = XRD at synchrotron source; DFT = density functional theory; TEM = transmission electron microscopy). The last row anticipates the result of this manuscript. Errors are given for $(d_{WZ} - d_{ZB})/d_{ZB}$ whenever available. The first interval refers to bounds for the statistic uncertainties, the second to bounds for the systematic uncertainties.

Reference	$(d_{WZ} - d_{ZB})/d_{ZB}$ (%)	Δ (nm)	l (μm)	S	C	T (K)	M
McMahon & Nelmes (2005)	$0.554^{+0.015}_{-0.015}$	Bulk	Bulk	–	–	–	SXRD
Yeh *et al.* (1992)	−1.3	–	–	–	–	–	DFT
Panse *et al.* (2011)	0.55	–	–	–	–	–	DFT
Tchernycheva *et al.* (2006)	0.52	10–35	0.25–0.45	$GaAs^{BL}_{111B}$	Au	570	TEM
Mariager *et al.* (2010)	$1.49^{+0.06}_{-0.06}$	75	0.5	$GaAs^{R}_{111B}$	Au	510	LXRD
Breuer (2011)	0.62	50	2.1	Si^{R}_{111}	Au	500	LXRD
Biermanns (2012)	$0.70^{+0.05}_{-0.05}$	90–285	0.02–1.2	Si^{NO}_{111}	Ga	580	SXRD
–	$0.66^{+0.02}_{-0.02-0.06}$	18–25	1.2–2.2	Si^{NO}_{111}	Ga	590	SXRD

lattice constants have been reported. Here, we focus on the ratio $(d_{WZ} - d_{ZB})/d_{ZB}$ of the distance between $(00.2)_w$ planes in wurtzite and $(111)_c$ planes in zinc blende structures.

Table 1 summarizes the known experimental and theoretical results for the ratio $(d_{WZ} - d_{ZB})/d_{ZB}$ for GaAs in free-standing nanowires and as bulk material. In the last row, we anticipate the result presented in this manuscript.

From this table, we see that the known values of this ratio span a wide range: the theoretical prediction of Yeh *et al.* (1992) for this ratio is −1.3% whereas Panse *et al.* (2011) estimate a value of 0.55% (although their absolute lattice constant of cubic GaAs disagrees with the experimental value by 0.8%). In the case of experimental data, values ranging from 0.52% up to 1.49% have been published (Biermanns *et al.*, 2011; Biermanns, 2012; Tchernycheva *et al.*, 2006; Mariager *et al.*, 2010; Breuer, 2011). Most notably, the following questions are of high relevance: (i) Does the ratio d_{WZ}/d_{ZB} in the nanowires change as a function of the diameter of the nanowires? (ii) Does the catalyst influence the ratio d_{WZ}/d_{ZB} in the grown nanowires? (iii) Does the substrate (material and particular preparation) influence the ratio d_{WZ}/d_{ZB}? (iv) Do the interplanar spacings d_{WZ} and d_{ZB} in the nanowires coincide with bulk material?

In this manuscript, we extract the ratio d_{WZ}/d_{ZB} of the interplanar spacing of the cubic $(111)_c$ planes and the wurtzite $(00.2)_w$ planes from X-ray measurements of thin self-catalyzed GaAs nanowires grown on $Si(111)_c$ substrates covered by native oxide. The most relevant difference of our samples to the samples investigated by Biermanns *et al.* (2011) and Biermanns (2012) is the much smaller diameter of the nanowires (see Table 1). Hence, we obtain information on the ratio d_{WZ}/d_{ZB} as a function of the diameter.

In contrast, the nanowires of Tchernycheva *et al.* (2006) feature similar diameters as our nanowires, but are grown on a different substrate and using gold as catalyst.

Specifically, we measured the vicinity of the 111_c reflection with a nanofocus set-up for various spatial positions on our samples. With the nanofocus set-up, we are able to separate the scattering from nanowires and parasitic growth ('crystallites'). As a consequence, we probe the ratio d_{WZ}/d_{ZB} of the nanowires exclusively. By combination with an absolute measurement of d_{WZ} as provided, for example, by Breuer (2011), we are able to compare the interplanar spacings d_{ZB} in the nanowires and in bulk ZB-GaAs.

We first describe the growth conditions of both samples in detail. Then, we summarize the results of post-growth *ex situ* scanning electron microscopy (SEM). Next, we describe our X-ray measurements and the evaluation thereof. Finally, we compare our ratio d_{WZ}/d_{ZB} of the interplanar distance of zinc blende and wurtzite in detail with the other measurements given in Table 1. During this discussion, we specifically address the questions (i) to (iv) mentioned above. For an investigation of the difference of the in-plane lattice spacings of both polytypes, we refer the reader to Biermanns *et al.* (2012*b*).

2. Description of the samples

Both samples have been grown in the portable molecular beam epitaxy system (Slobodskyy *et al.*, 2012) of the synchrotron source ANKA at KIT in Karlsruhe, Germany. As substrate, p-doped $Si(111)_c$ with a thin native oxide layer has been used. Before growth, the substrates had been heated to T_{Sub} = 750°C in order to evaporate residuals from the substrate surface. Then, the substrate temperature was changed to T_{Sub} = 590°C and the As shutter was opened. Opening of the Ga shutter 5 min later (background pressure of 2.9×10^{-7} mbar) initiated the growth of the nanowires (definition of growth time t_{Growth} = 0 min).

Sample 1 was grown at a V/III ratio of $r_{V/III} \simeq 3.3$. The corresponding Ga flux is equivalent to a nominal two-dimensional GaAs layer growth-rate of g_{GaAs} = 46 nm h^{-1} on $GaAs(001)_c$. For sample 2, the respective values are $r_{V/III} \simeq 4.9$ and g_{GaAs} = 30 nm h^{-1}. The V/III ratio has been calibrated from the reflection high-energy electron diffraction (RHEED) pattern using a $GaAs(001)_c$ substrate at T_{Sub}. Specifically, we monitored the transition from the (2×4) to the (4×2) surface reconstruction.

After t_{Growth} = 60 min in the case of sample 1 and t_{Growth} = 30 min in the case of sample 2, the Ga and As shutters were

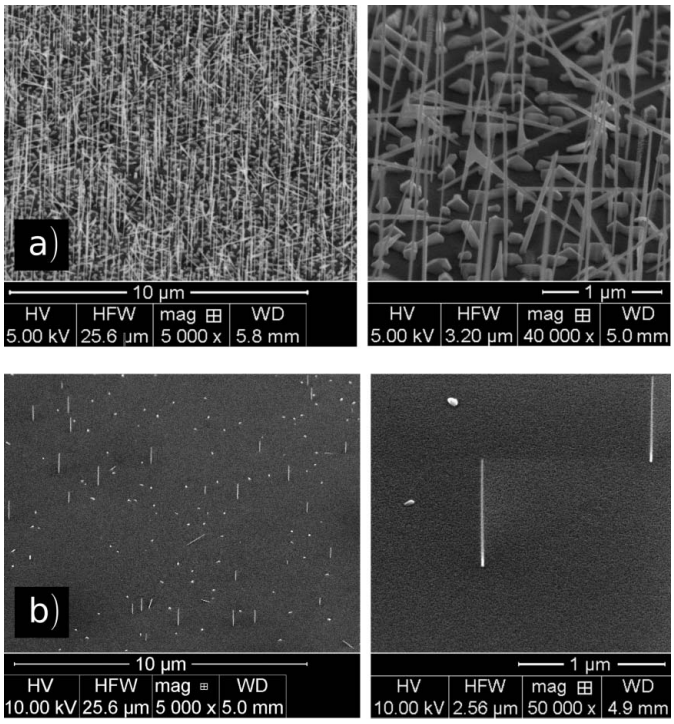

Figure 2
SEM images of the measured samples [sample 1 in (*a*), sample 2 in (*b*)]. The left-hand images give an overview over a wide area of the samples whereas the right-hand images are taken at a much higher magnification.

closed simultaneously. Heating of the substrate was stopped, and its temperature was ramped down to 100°C in 8 min.

In Fig. 2, post-growth *ex situ* SEM images of both samples are depicted. The results of the post-growth *ex situ* characterization by means of SEM are summarized in Table 2. If we combine the mean volume of the nanowires and crystallites with the mean densities of these objects, we find that approximately 15% (sample 1) and 8.4% (sample 2) of the GaAs material constitutes nanowires. Given the mean height of the nanowires and their small diameter as extracted from the SEM analysis, we will neglect the effect of the strain induced by the substrate during the evaluation of our X-ray measurements (Biermanns *et al.*, 2012*a*,*b*; Davydok *et al.*, 2012).

Table 2
Summary of the post-growth *ex situ* SEM evaluation.

Physical quantity (unit)	Sample 1	Sample 2
Nanowire number density (μm^{-2})	2.2	0.064
Nanowire mean height (µm)	2.22	1.15
Nanowire height distribution width (µm)	0.04	0.20
Nanowire mean diameter (nm)	25	18
Nanowire mean volume (μm^3)	1.1×10^{-3}	2.9×10^{-4}
Crystallites number density (μm^{-2})	5.3	0.56
Crystallites mean volume (μm^3)	2.7×10^{-3}	3.6×10^{-4}

3. Experimental details of the X-ray measurements at ID13 at ESRF

The measurements were performed at beamline ID13 of the European Synchrotron Radiation Facility (ESRF) in Grenoble, France, under nanofocus conditions providing a Gaussian beam profile with a full width at half-maximum of 250 nm. The energy of the incident X-ray radiation was 14.9 keV. Only the reflections hhh_c feature a non-zero component of the momentum transfer in the $[111]_c$ direction and have been accessible at beamline ID13 at the ESRF due to its experimental constraints. The GaAs signal for reflections $h > 1$ was too weak to be detected for our thin nanowires (the 222_c reflection of GaAs is quasi-forbidden). Thus, we were limited to measuring the 111_c Bragg reflection of GaAs.

The intensity distribution near the 111_c Bragg reflection of GaAs was recorded with a two-dimensional Maxipix detector which was placed at a fixed spatial position (distance to sample ~0.67 m). The incidence and exit angle α_i and α_f of the X-ray beam have been set such that the Ewald sphere intersects the crystal truncation rod (CTR) of the Si substrate close to the 111_c GaAs signal. Consequently, a single two-dimensional detector image in our arrangement records a part of the Ewald sphere which essentially corresponds to the q_y–q_z plane in reciprocal space (see Fig. 3). For our purpose, we focus on the intensity distribution along the q_z direction since it directly reveals information about the interplanar spacings of the $(111)_c$ as well as the $(00.2)_w$ planes.

Keeping these conditions of the set-up, the sample was scanned (stepwise) by a nanostage in the *x*- and *y*-direction in such a way that the illuminated areas of the samples are disjoint. At each position the detector image was recorded. All

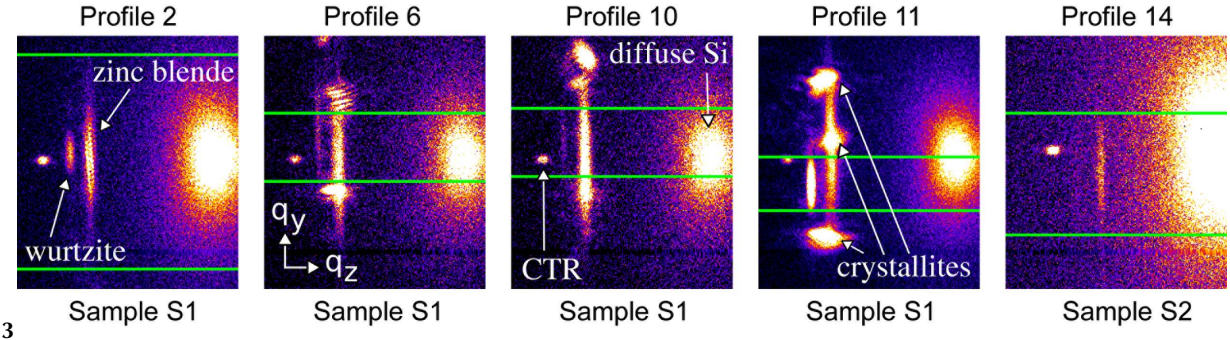

Figure 3
The five detector frames suited best for determining the ratio of the interplanar distance of wurtzite and zinc blende structures in our self-catalyzed GaAs. From suitable regions of interest (q_y range inside the green lines), the q_z profiles in Fig. 6 have been derived.

these detector images show diffuse scattering of silicon substrate and a part of the crystal truncation rod (CTR) of the substrate. Some images show a signal close to the GaAs Bragg peak in addition (see Fig. 3). In some of these cases, part of a single crystallite or a single nanowire has been illuminated. Depending on the nanowire and crystallite densities, multiple GaAs nano-objects have been illuminated at the same time (*e.g.* Fig. 3). The latter case is particularly important in the case of sample 1 which has a higher density of GaAs nanostructures than sample 2. In contrast, the signals of sample 2 typically stem only from a single GaAs nano-object, but are much weaker than in the case of sample 1 due to the smaller illuminated volume of crystalline GaAs.

4. Evaluation of the X-ray data

Since we aim to extract crystalline information in the $[111]_c$ direction, we integrate the frames in the q_y direction. We then fit a Pearson VII function to the silicon peak and thereby obtain the center of the diffuse silicon signal in the q_z direction. After this, we shift the q_z profiles of each frame in such a way that the silicon center is zero. Since the center is, in general, a non-integer value, linear interpolation of the shifted data is performed in order to maintain identical q_z positions of all data sets. Since the GaAs signal is located at lower q_z values than silicon, the GaAs signal is thereby shifted to negative values. By this procedure, we will also be able to investigate and compare the cumulative signal of different scans (see Figs. 4 and 5).

For estimation of the ratio of the interplanar spacings of Ga (or As) planes of both polytypes in the nanowires, we will express the splitting of wurtzite and zinc blende in reciprocal space as a fraction s of the distance from zinc blende GaAs to the center of the silicon signal, *i.e.*

$$s = \frac{q_{ZB} - q_{WZ}}{q_{Si} - q_{ZB}}. \quad (1)$$

Then, the ratio of the interplanar spacings of Ga (or As) planes is

$$\begin{aligned}\frac{d_{WZ}}{d_{ZB}} = \frac{q_{ZB}}{q_{WZ}} &= \frac{1}{1-(q_{ZB}-q_{WZ})/q_{ZB}} = \left[1 - \frac{s(q_{Si}-q_{ZB})}{q_{ZB}}\right]^{-1} \\ &= \left[1 - s\left(\frac{d_{ZB}-d_{Si}}{d_{Si}}\right)\right]^{-1} = \left[1 - s\left(\frac{a_{ZB}-a_{Si}}{a_{Si}}\right)\right]^{-1} \\ &\approx 1 + s\left(\frac{a_{ZB}-a_{Si}}{a_{Si}}\right). \quad (2)\end{aligned}$$

If we assume that the lattice spacing of the $(111)_c$ planes of zinc blende in GaAs nanowires is identical to its bulk value and employ $a_{ZB}^{GaAs} = 5.65325$ Å and $a_{Si} = 5.43102$ Å, then $(a_{ZB} - a_{Si})/a_{Si} = 4.092\%$.

By the introduction of the quantity s as defined in equation (1), we gain two advantages. First, we circumvent a calibration of the q_z axis. Therefore, we are sure that our results are not falsified by calibration errors. Second, the values of s are independent of the absolute values of a_{ZB}^{GaAs} and a_{Si}. As a consequence, we do not label our axis in the q_z direction in our plots by absolute q_z-values, but by s and the pixel distance to the silicon center. For simplicity, we still refer to this axis as the q_z axis.

Table 3
Details on the classification of our acquired detector frames.

Scan	1	2	3	Sum
Total frames	36	112	112	260
Wire frames	6	16	19	41
Crystallite frames	16	32	37	85

In order to discuss the signal of the nanowires and crystallites separately, we classified our detector frames by manual inspection. Based on the results of our SEM investigations (see Fig. 2 and Table 2) and the FWHM of our focused X-ray beam, we expect signals from the nanowires to exhibit large aspect ratios $\Delta q_y/\Delta q_z$ (up to 15). In contrast, signals from the crystallites correspond to aspect ratios $\Delta q_y/\Delta q_z$ similar to unity. Consequently, detector frames which exhibit scattering signals with either only high aspect ratios or only aspect ratios smaller or similar to unity are classified as either 'wires' or 'crystallites', respectively. We point out that we do not require that the GaAs signal on a detector frame originates from the scattering of a single GaAs nano-object only. We only require for our classification that a detector frame contains scattering of one class of GaAs objects.

For sample 1, we found 194 frames which mainly originate from wire scattering and 27 frames which mainly originate from crystallites. For sample 2, we sorted the data of scans of three different spatial grids on the sample. These three scans were performed at three different positions on the substrate separated by approximately 1 mm. At each position, a fine rectangular grid of an area of approximately 120 µm × 150 µm was scanned with a stepping of the order of 20 µm. The outcome of the classification of the detector frames of the three scans of sample 2 is given in Table 3.

We now first look at the cumulative signal of the nanowires and crystallites for both samples. We would like to point out that such a separation of the two contributions has only been possible due to a nanofocus set-up, as provided by ID13 at ESRF. This ability to separate these two contributions provides valuable insights and information for proper understanding and interpretation of ensemble-averaged measurements without a nanofocused beam, in particular for time-resolved *in situ* X-ray measurements as presented by Schroth *et al.* (2014).

We summed all these profiles of each class 'wires', 'crystallites' and 'all' for both samples. The category 'all' also contains those frames without scattering signal of the GaAs nanostructures on the detector as well as those frames which exhibit scattering of wires and crystallites on the same detector image. This way, we obtain the one-dimensional q_z profiles for both samples which are depicted in Fig. 4. The three curves of each sample have been normalized to exhibit identical behavior of the diffuse silicon background before subtraction of the diffuse silicon background. However, for better comparison of both samples, the curves of sample 2

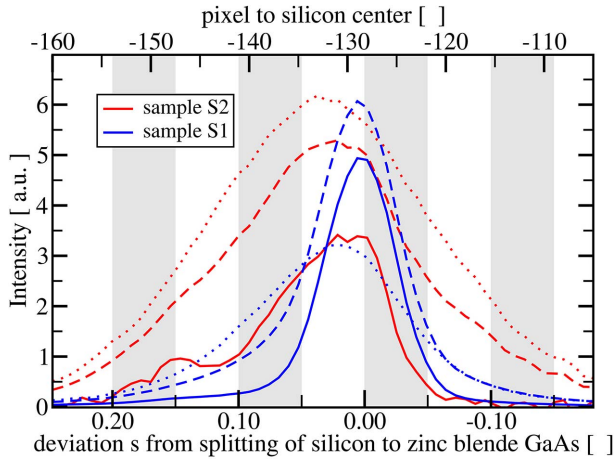

Figure 4
Comparison of the cumulative q_z intensity profiles of sample S1 (blue) and S2 (red). Dotted lines correspond to the signal of the crystallites of the respective sample, continuous lines to the wire signal and dashed lines to the overall signal of all observed frames.

have been multiplied with the same factor such that the maximum of the strongest signal of both samples is approximately equal (*i.e.* overall signal for sample 1, crystallite signal for sample 2). We observe that the profile of the signal from the crystallites is almost equal for both samples. However, the characteristics of the wire signal differs strongly between sample 1 and sample 2: for sample 1, the cumulative nanowire signal shows a single peak with no fine structure centered approximately at a distance of 128 pixels from silicon; for sample 2, we observe a highly asymmetric peak approximately at a distance of 129 pixels to the maximum of the diffuse silicon cloud and a second, small, peak with the distance to silicon close to 148 pixels.

We now discuss these q_z profiles in greater detail. If all wires were built by one polytype only ('perfect phase purity'), we would expect a single peak centered around the q_z position for the respective polytypes every time we illuminate a fraction of a wire with our nanofocus. Since our nanofocus has a beam size of 250 nm and we illuminate at angles of approximately 8°, the width of such a peak in the q_z direction is much smaller than the splitting of the signal in the q_z direction which is expected from the results summarized in Table 1. If we now consider wires with both polytypes, but transitions from one polytype to the other are very unlikely ('high phase purity'), we still observe a single peak centered around the q_z position for the respective polytype on each frame in most cases. The summation of all nanowire frames now reveals two well separated peaks at the positions of the pure polytypes. Their relative weight equals the fractions of the polytypes. In some cases, we illuminate domains of both polytypes at the same time, either in different wires or if the interface of two extended polytype segments is located close to the center of the beam. The former case is more relevant for sample 1 (high wire density) whereas the latter case is of higher relevance for sample 2 (low wire density). In such cases, two separated peaks are even observed on a single detector frame (see Fig. 3).

For a highly random stacking without extended segments of defect-free stacking of either polytype (very low phase purity), only a single narrow peak is observed in the cumulative signal. Thus, a single narrow peak is no indication for wires with low stacking fault density. Its center of mass is located according to the phase fractions of the polytypes. For equal fractions of both polytypes, the center of mass of this peak is the center of the positions of the pure polytypes. Consequently, intensity between the positions of the pure polytypes (other than the tails of the peaks at the positions of the pure polytype) indicates that regions with low phase purity are present in the nanowires. Therefore, the nanowires in sample 2 exhibit both polytypic phases. In consequence, we focus on sample 2 for the extraction of the ratio d_{WZ}/d_{ZB} from the cumulative signal.

A more sophisticated discussion of the q_z profiles of the 111_c Bragg reflection of polytypic GaAs nanowires based on a Markov model for the stacking sequences in an ensemble of nanowires is presented by Schroth *et al.* (2014).

In Fig. 5 the q_z profiles of our three scans on different spatial grids of sample 2 are depicted. Here, the normalization of different scans and the sum thereof is such that the weight of the crystallites is equal. Whereas the signal of the crystallites is almost equal for all three scans, fluctuations from scan to scan are observed in the wire signal. Nevertheless, scan 2 exhibits two clear peak positions, a peak close to position $p_1 = (-128.0 \pm 1.0)$ pixel and a second peak close to $p_2 = (-148.0 \pm 1.5)$ pixel. Based on the above discussion, we attribute the first peak to the zinc blende position and the latter peak to the wurtzite position. The intensity between these two positions stems from illumination of wire segments with very low phase purity. The uncertainty of the second peak (1.5 pixel) is higher due to the higher width of the peak along q_z and its reduced height in comparison with the first peak (1.0 pixel).

Scan 1 also shows a peak at position −128.0 pixel, but a lot of weight is shifted inside the range [−148 pixel, −128 pixel]. In combination with the low number of wires in scan 1, the second peak at position −148 pixel cannot be resolved. For

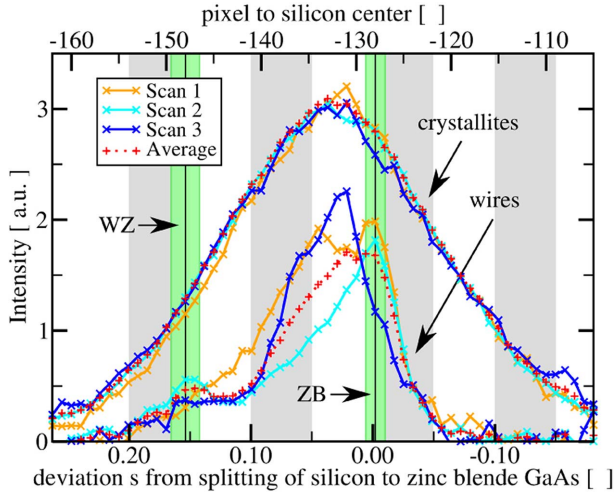

Figure 5
Cumulative q_z intensity profile of wires and crystallites of three different scans of the sample S2. Scans are marked by color.

scan 3, we observe that the peak close to position −128 pixel is shifted inside this range. Consequently, within the fragments of the nanowires illuminated by that scan, most fragments contained short segments of wurtzite which results in a slightly increased mean lattice constant. Nevertheless, a plateau of the scattered intensity is observed in the range [−149 pixel, −143 pixel]. This is also compatible with the second peak located at (−148.0 ± 1.5) pixel. These differences of scans 1–3 indicate high fluctuations of the local phase purities and phase fractions of the wires and characterization of these properties should rely on methods with high statistical significance (Schroth *et al.*, 2014). In contrast, the extraction of the ratio d_{WZ}/d_{ZB} *in the nanowires* was only possible due to the highly focused beam which permits the separation of the contributions from nanowires and crystallites.

If we consider these two sub-peaks p_1 and p_2, we extract a splitting s of wurtzite and zinc blende phase [see equation (1)] corresponding to $s_E = 15.6\% \pm 1.9\%$ of distance of the zinc blende peak to silicon which implies

$$(d_{WZ}/d_{ZB})_E \overset{\text{Eq.2}}{=} 1 + 0.64\% \pm 0.08\%. \qquad (3)$$

Since these cumulative q_z profiles contain also those frames which do not correspond to illumination of very pure phase segments of either (or both) polytypes, we now turn to evaluation of a selected subset of our measured detector frames. More specifically, we selected the best 20 candidates from our set of detector frames which contain typical wire signals inside a suitable region of interest (as exemplary shown in Fig. 3) and show a two-peak splitting after subtraction of the background (Pearson VII, as before). If both sub-peaks have no fine structure and are clearly separated, *i.e.* almost no photon counts between the two sub-peaks, it is highly likely that we hit very pure segments of both polytypes (either in one wire or of different wires). The last requirement is very important since such counts indicate that the illuminated structures are most likely not as pure as required: the mean lattice constant of the illuminated structures is likely to differ from the pure structures. This would result in a drift of one or both subpeaks towards each other. Therefore, such candidates systematically underestimate the splitting of wurtzite and zinc blende. From these 20 candidates for determining the splitting of the two subpeaks as well as the positions of zinc blende GaAs, we selected in a second step the best five q_z profiles which have been depicted in Fig. 3 together with the respective regions of interest (q_y range inside the green lines). This selection of the five best candidates was based on the requirements of sufficient signal-to-noise ratio, almost Gaussian shape of both subpeaks and, finally, as few counts as possible in the intermediate domain.

All 20 candidates were then fitted by the sum of two Gaussian distributions. If photons have been counted in the region between the two subpeaks, some data points in that region have been ignored in the two Gaussian fits and, thereby, partially compensating the above-mentioned drift towards each other. However, no data points have been ignored for the five best candidates in Fig. 6.

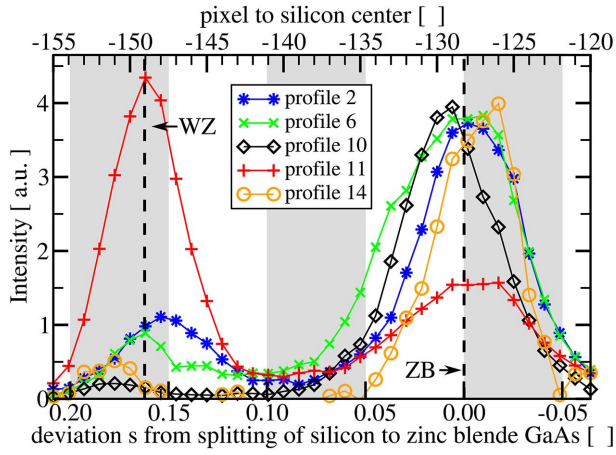

Figure 6
q_z intensity profiles of the five frames suited best for determining the ratio of the interplanar spacing of wurtzite and zinc blende structures (see Fig. 3). The dashed vertical lines correspond to $s = 16.2\%$ which, in turn, corresponds to $(d_{WZ}/d_{ZB}) = 1 + 0.66\%$.

The extracted splittings of these two Gaussians are summarized in Fig. 7. Clearly, most 'non-optimal' candidates indicate systematically a smaller splitting than the value retrieved from the five best profiles.

The (weighted) mean values

$$\mu = \sum_i w_i x_i, \qquad w_i = \frac{e_i^{-1}}{\sum_j e_j^{-1}}, \qquad (4a)$$

for the splitting and the error

$$\sigma = \left[(1/N)\sum_i w_i (x_i - \mu)^2\right]^{1/2} \qquad (4b)$$

thereof are included as horizontal lines for the best five profiles (orange) and for all 20 profiles (green). Here, e_i refers to the error of the value x_i from profile i. Note that σ refers to the error of the mean value μ and not to an intrinsic width of a distribution. The extracted values for the splitting of wurtzite

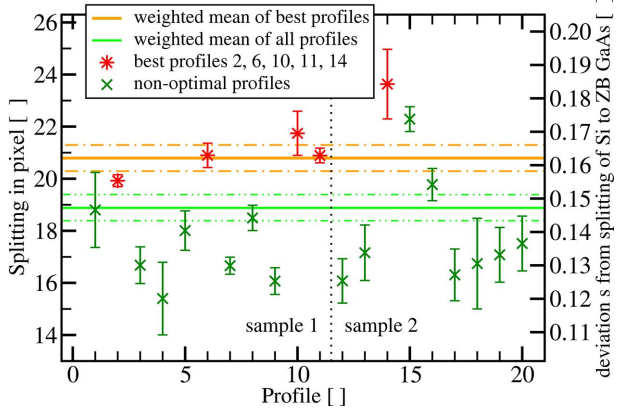

Figure 7
Splitting of the two subpeaks in reciprocal space resulting from the different interplanar distance of zinc blende and wurtzite GaAs. The five best profiles (see Fig. 6) are highlighted by red stars. The other candidates are likely to underestimate the splitting of the position of pure zinc blende and wurtzite GaAs (see discussion in main text).

and zinc blende signal are $\mu_5 \pm \sigma_5 = (20.79 \pm 0.50)$ pixel and $\mu_{20} \pm \sigma_{20} = (18.88 \pm 0.49)$ pixel. An identical evaluation for the zinc blende position of GaAs yields $\mu_{ZB} \pm \sigma_{ZB} = (128.25 \pm 0.28)$ pixel which is employed for the calibration of the *s*-axis in Figs. 4, 5 and 6. Consequently, the fraction *s* in equation (1) is

$$s_5 = 16.2\% \pm 0.4\%, \quad (5a)$$

$$s_{20} = 14.7\% \pm 0.4\%. \quad (5b)$$

which, by equation (2), implies

$$(d_{WZ}/d_{ZB})_5 = 1 + 0.66\% \pm 0.02\%, \quad (6a)$$

$$(d_{WZ}/d_{ZB})_{20} = 1 + 0.60\% \pm 0.02\%. \quad (6b)$$

The value $(d_{WZ}/d_{ZB})_5$ is very similar to the value which we obtained from the cumulative wire signal $(d_{WZ}/d_{ZB})_E$ given in equation (3). $(d_{WZ}/d_{ZB})_{20}$ is shifted towards a slightly smaller value due to the discussed systematic errors. Nevertheless, it imposes a lower bound on the ratio d_{WZ}/d_{ZB} with high statistical significance and, thus, is of importance for comparison with other measurements (see Table 1).

5. Comparison with literature

Within the error margins, our value is fully compatible with the value obtained by Biermanns *et al.* (2011) and Biermanns (2012) where a relative increase of interplanar spacing in the $[111]_c$ direction of wurtzite phase of $0.70\% \pm 0.05\%$ has been observed for nanowires with diameters in the range from (90 ± 8) nm to (285 ± 65) nm. Since our wires are also grown self-assisted on (111) oriented silicon substrates covered by native oxide at very similar growth temperatures, our thin wires with diameters down to $\sim$18 nm indicate that the interplanar spacing of wurtzite and zinc blende phase in the $[111]_c$ direction is independent of the nanowire diameter at least in the range from 18 nm to 300 nm.

Next, we compare our result with the spacing d_{WZ} obtained by Breuer who measured a high-resolution X-ray diffraction (XRD) profile of the vicinity of the 111_c Bragg reflection (with a triple crystal setup and a laboratory X-ray source) for pencil-shaped gold-catalyzed GaAs nanowires which consist essentially of wurtzite only [Fig. 3.7 of Breuer (2011)]. Their main diameters were around 50 nm; the tip diameters ranged from 10 nm to 20 nm. Thus, the diameters are in the above range for which the ratio d_{WZ}/d_{ZB} is independent of the diameter. From these measurements, Breuer derived the absolute value d_{WZ} = 3.284 Å for the spacing of the $[00.2]_w$ planes in their GaAs wurtzite nanowires. If we compare this value with the bulk value of zinc blende GaAs, $a_{ZB}^{(GaAs)} = 5.65325$ Å, we obtain the ratio $d_{WZ}/d_{ZB} = 1 + 0.62\%$. Like the result of Biermanns *et al.* (2011) and Biermanns (2012), this value is compatible with our results: it is larger than our lower bound $(d_{WZ}/d_{ZB})_{20}$ and also close to our best estimate $(d_{WZ}/d_{ZB})_5$. Consequently, within our error margins and based on the assumption that the lattice constant of zinc blende GaAs in nanowires and bulk material is equal, we observe no influence of the gold catalyst or the removal of the native oxide layer on the ratio d_{WZ}/d_{ZB}.

At this point we come back to equations (1) and (2). For extraction of the ratio *s* from our experimental data, we do not assume that the spacing d_{ZB} in the nanowires is equal to its respective bulk value. This assumption is only employed for translation of *s* to the ratio d_{WZ}/d_{ZB}. If we reformulate equation (2) as

$$d_{ZB} = \frac{d_{WZ}\, d_{Si}\,(1+s)}{d_{Si} + s\, d_{WZ}}, \quad (7)$$

we are able to extract information about the zinc blende spacing d_{ZB} *in the nanowires*, since an absolute value for d_{WZ} in the nanowires and an estimate for *s* specific for the nanowires (due to the nanofocus setup) is known. We point out that typically absolute direct measurements of d_{ZB} in the nanowires are very difficult either due to parasitic growth of strained GaAs structures for silicon substrates or the substrate signal for GaAs substrates.

If we employ d_{WZ} = 3.284 Å from Breuer (2011) and assume that the ratio d_{WZ}/d_{ZB} is neither influenced by the gold catalyst nor the native oxide layer (*instead* of the assumption that d_{ZB} in bulk zinc blende GaAs is equal to d_{ZB} in nanowires), we can *deduce* from our results bounds on the deviation of d_{ZB} in bulk material and nanowires. If we exploit s_5 and s_{20} [see equation (5)], the spacing d_{ZB} differs from the bulk value $d_{ZB}^{(bulk)} = a_{ZB}^{(bulk)}/\sqrt{3}$ by only -0.04% and 0.01%, respectively.

We point out that the result for the ratio d_{WZ}/d_{ZB} in nanowires given in this manuscript and by Biermanns *et al.* (2011), Biermanns (2012) and Breuer (2011) is larger than for bulk GaAs [see McMahon & Nelmes (2005) for an experimentally obtained value and Panse *et al.* (2011) for a recent *ab initio* DFT+LDA prediction in Table 1].

Only the result given by Tchernycheva *et al.* (2006) is close to the ratio d_{WZ}/d_{ZB} of bulk GaAs. These authors retrieved their interplanar spacing of d_{WZ} = 3.281 Å ($c_{WZ} = 2d_{WZ}$ = 6.562 Å) from the inter-spot distance of transmission electron microscopy (TEM) diffraction patterns of gold-catalyzed GaAs nanowires grown on (111)B oriented GaAs substrates. If we compare this with $d_{ZB} = a_{ZB}/\sqrt{3} = 3.26391$ Å (bulk zinc blende GaAs), it corresponds to an increase of the interplanar spacing of 0.52%, very similar to the bulk values for the ratio d_{WZ}/d_{ZB} [see the references McMahon & Nelmes (2005) and Panse *et al.* (2011) in Table 1].

These bulk ratios and the nanowire ratio from Tchernycheva *et al.* (2006) are smaller by approximately 20% than our value $(d_{WZ}/d_{ZB})_5 - 1$. Even if we consider our lower bound $(d_{WZ}/d_{ZB})_{20} - 1$, their values are still approximately 10% smaller than our result. However, Tchernycheva *et al.* (2006) and Panse *et al.* (2011) did not provide an error estimate for their result.

Finally, Mariager *et al.* (2010) extracted an interplanar spacing of $d_{WZ} = (3.3125 \pm 0.002)$ Å for gold-catalyzed GaAs nanowires on (111)B-oriented GaAs substrates. Hence, the bulk reference d_{ZB} corresponds to an increase of the interplanar spacing of $(d_{WZ}/d_{ZB}) = 1 + 1.49\% \pm 0.06\%$, although

they could not observe any difference of the in-plane lattice parameter of zinc blende and wurtzite GaAs structures. This value is more than twice as large as our result and the other values given in Table 1. Since their diameter is larger than for our samples and the samples investigated by Breuer (2011) and Tchernycheva *et al.* (2006), but smaller than the samples of Biermanns *et al.* (2011) and Biermanns (2012), the large ratio $(d_{WZ}/d_{ZB}) = 1 + 1.49\% \pm 0.06\%$ cannot be explained by a dependence on the diameter of the nanowire. Moreover, two samples grown with gold as catalyst have ratios $(d_{WZ}/d_{ZB}) \leq 1 + 0.62\%$ (see Table 1). One of these samples has also been grown on a (111)B-oriented GaAs substrate (but a buffer layer was grown first). We are unable to explain this large value (d_{WZ}/d_{ZB}) without further research on GaAs nanowires grown on GaAs-111 substrates.

6. Conclusion

In conclusion, we extracted the ratio d_{WZ}/d_{ZB} of the interplanar lattice spacing of $(00.2)_w$ wurtzite and $(111)_c$ zinc blende planes in thin freestanding self-catalyzed GaAs nanowires grown on (111) oriented silicon substrates (covered by native oxide) based on X-ray measurements of the 111_c Bragg reflection obtained with a nanofocus beam.

Our result $d_{WZ}/d_{ZB} = 1 + 0.66\% \pm 0.02\%$ is consistent with the values given by Biermanns *et al.* (2011), Biermanns (2012) and Breuer (2011) for nanowires with significantly larger diameters. Thus, these results indicate that the interplanar spacing of wurtzite and zinc blende phase in the $[111]_c$ direction is independent of the nanowire diameter (at least) in the range from approximately 20 nm to 300 nm.

By the use of the nanofocus set-up at ID13 at ESRF, the scattering from nanowires could be separated from the scattering of other crystalline structures. Thus, our result for the ratio d_{WZ}/d_{ZB} is specific for the nanowires only and is larger than its value in bulk GaAs.

The ratios d_{WZ}/d_{ZB} for GaAs nanowires grown on Si-111 substrates (with and without Gold as catalyst) are consistent. However, the ratios for GaAs nanowires grown on GaAs-(111)B substrates deviate to smaller (Tchernycheva *et al.*, 2006) as well as larger (Mariager *et al.*, 2010) values, beyond the error margins of the results for Si-111. Consequently, additional measurements for GaAs nanowires on GaAs-(111)B substrates are needed in the future.

We are grateful to M. Burghammer, M. Sztucki and E. Di Cola for providing assistance in using the beamline ID13 at the European Synchrotron Radiation Facility (ESRF), Grenoble, France, where we performed the presented X-ray measurements. Moreover, we acknowledge the support by Hans Gräfe, Bärbel Krause and Svetoslav Stankov in the UHV laboratory at the Institute of Photon Science and Synchrotron Radiation, KIT, and by Delphine Chassaing and Robby Prang at the Institute of Nanotechnology, KIT. Moreover, we are grateful for the support of Claudia Herrmann and Hans-Peter Schönherr at Paul-Drude-Institut für Festkörperelektronik in Berlin. The portable MBE project and the laboratory instrumentation was financed by the BMBF project 05ES7CK, and by the German excellence initiative within the project KIT Nanolab@ANKA. Moreover, this work was supported by the ongoing BMBF project 05K13PS3 and Deutsche Forschungsgemeinschaft (DFG) under grants Pi 217/38 and Ge 2224/2.

References

Bao, J., Bell, D. C., Capasso, F., Wagner, J. B., Mårtensson, T., Trägårdh, J. & Samuelson, L. (2008). *Nano Lett.* **8**, 836–841.
Biermanns, A. (2012). PhD thesis, Universität Siegen, Germany.
Biermanns, A., Breuer, S., Davydok, A., Geelhaar, L. & Pietsch, U. (2011). *Phys. Status Solidi*, **5**, 156–158.
Biermanns, A., Breuer, S., Davydok, A., Geelhaar, L. & Pietsch, U. (2012*a*). *J. Appl. Cryst.* **45**, 239–244.
Biermanns, A., Breuer, S., Trampert, A., Davydok, A., Geelhaar, L. & Pietsch, U. (2012*b*). *Nanotechnology*, **23**, 305703.
Breuer, S. (2011). PhD thesis, Humboldt-Universität Berlin, Germany.
Cartwright, J. (2010). *Nature News*, doi:10.1038/news.2010.694.
Cui, Y., Wei, Q., Park, H. & Lieber, C. M. (2001). *Science*, **293**, 1289–1292.
Davydok, A., Breuer, S., Biermanns, A., Geelhaar, L. & Pietsch, U. (2012). *Nanoscale Res. Lett.* **7**, 109.
Dick, K. A., Caroff, P., Bolinsson, J., Messing, M. E., Johansson, J., Deppert, K., Wallenberg, L. R. & Samuelson, L. (2010). *Semiconductor Sci. Technol.* **25**, 024009.
Duan, X., Huang, Y., Agarwal, R. & Lieber, C. M. (2003). *Nature (London)*, **421**, 241–245.
Hayden, O., Agarwal, R. & Lu, W. (2008). *Nano Today*, **3**, 12–22.
Hjort, M., Lehmann, S., Knutsson, J., Timm, R., Jacobsson, D., Lundgren, E., Dick, K. & Mikkelsen, A. (2013). *Nano Lett*, **13**, 4492–4498.
Hochbaum, A. I., Chen, R., Delgado, R. D., Liang, W., Garnett, E. C., Najarian, M., Majumdar, A. & Yang, P. (2008). *Nature (London)*, **451**, 163–167.
Koguchi, M., Kakibayashi, H., Yazawa, M., Hiruma, K. & Katsuyama, T. (1992). *Jpn. J. of Appl. Phys.* **31**, 2061.
McMahon, M. I. & Nelmes, R. J. (2005). *Phys. Rev. Lett.* **95**, 215505.
Mariager, S. O., Lauridsen, S. L., Sørensen, C. B., Dohn, A., Willmott, P. R., Nygård, J. & Feidenhans'l, R. (2010). *Nanotechnology*, **21**, 115603.
Mourik, V., Zuo, K., Frolov, S. M., Plissard, S. R., Bakkers, E. P. A. M. & Kouwenhoven, L. P. (2012). *Science*, **336**, 1003–1007.
Panse, C., Kriegner, D. & Bechstedt, F. (2011). *Phys. Rev. B*, **84**, 075217.
Reimer, M. E., Bulgarini, G., Akopian, N., Hocevar, M., Bavinck, M. B., Verheijen, M. A., Bakkers, E. P. A. M., Kouwenhoven, L. P. & Zwiller, V. (2012). *Nat. Commun.* **3**, 737.
Saxena, D., Mokkapati, S., Parkinson, P., Jiang, N., Gao, Q., Tan, H. H. & Jagadish, C. (2013). *Nat. Photon.* **7**, 963–968.
Schroth, P., Köhl, M., Hornung, J.-W., Dimakis, E., Somaschini, C., Geelhaar, L., Biermanns, A., Bauer, S., Lazarev, S., Pietsch, U. & Baumbach, T. (2014). Submitted.
Slobodskyy, T., Schroth, P., Grigoriev, D., Minkevich, A. A., Hu, D. Z., Schaadt, D. M. & Baumbach, T. (2012). *Rev. Sci. Instrum.* **83**, 105112.
Spirkoska, D., Arbiol, J., Gustafsson, A., Conesa-Boj, S., Glas, F., Zardo, I., Heigoldt, M., Gass, M. H., Bleloch, A. L., Estrade, S., Kaniber, M., Rossler, J., Peiro, F., Morante, J. R., Abstreiter, G., Samuelson, L. & Fontcuberta i Morral, A. (2009). *Phys. Rev. B*, **80**, 245325.
Stern, E., Klemic, J. F., Routenberg, D. A., Wyrembak, P. N., Turner-Evans, D. B., Hamilton, A. D., LaVan, D. A., Fahmy, T. M. & Reed, M. A. (2007). *Nature (London)*, **445**, 519–522.

Tchernycheva, M., Harmand, J. C., Patriarche, G., Travers, L. & Cirlin, G. E. (2006). *Nanotechnology*, **17**, 4025.
Tian, B., Zheng, X., Kempa, T. J., Fang, Y., Yu, N., Yu, G., Huang, J. & Lieber, C. M. (2007). *Nature (London)*, **449**, 885–889.
Tomioka, K., Tanaka, T., Hara, S., Hiruma, K. & Fukui, T. (2011). *IEEE J. Select. Topics Quantum Electron.* **17**, 1112–1129.
Tomioka, K., Yoshimura, M. & Fukui, T. (2012). *Nature (London)*, **488**, 189–192.
Xiang, J., Lu, W., Hu, Y., Wu, Y., Yan, H. & Lieber, C. M. (2006). *Nature (London)*, **441**, 489–493.
Yeh, C.-Y., Lu, Z. W., Froyen, S. & Zunger, A. (1992). *Phys. Rev. B*, **46**, 10086–10097.